Dual Functional Alginate and Collagen-Based Injectable Hydrogel for Treatment of Cancer and Its Metastasis

Juyoung Hwang
Fudan University
Eun-Koung An
Yeungnam University
Wei Zhang
Fudan University
Jun-O Jin (jinjo@yu.ac.kr)
Fudan University

Research Article

Keywords: Thermal responsive gel, Photothermal therapy, Immunotherapy, Cancer metastasis, Tumor recurrence

Posted Date: February 21st, 2022

DOI: https://doi.org/10.21203/rs.3.rs-1356801/v1

Abstract

Background

For prevention of recurrence and metastasis, immunotherapies against cancer has been gaining attention. Cancer immunotherapy can induce memory immunity against cancer antigens which selectively kills the cancer. However, there are difficulties for inducing cancer antigen-specific immune activity due to limited cancer antigen. In this study, we synthesized dual functional hydrogel for inducing antigen generation and immune activation.

Methods

To elicit cancer self-antigen specific immune activation, we synthesized an alginate-collagen-based injectable hydrogel, called thermal responsive hydrogel (pTRG), incorporated with indocyanine green and immune stimulator polyinosinic:polycytidylic acid (poly I:C). pTRG was evaluated for its anticancer and anti-metastatic effects against CT-26 carcinoma and 4T1 breast tumor in mice by combining photothermal therapy (PTT) and immunotherapy.

Results

Irradiation of near-infrared (NIR) promoted elevation of temperatures in the pTRG, consequently promoting the therapeutic effect of tumors in mice. The cured mice from the CT-26 tumor challenged by pTRG prevented the second challenge of metastatic cancer growth in the lung mediated by cancer antigen-specific T cell immunity. Moreover, in 4T1 tumors, one of the candidate tumor models for PTT, pTRG successfully treated 1st challenged tumor by PTT and inhibited the second challenge of 4T1 tumor growth in the lung. To further evaluate the carrier function of TRGs, different types of immunotherapeutic molecules were incorporated into TRGs and showed effective elimination against the first challenged CT-26 tumor and prevention of second challenge metastatic cancer growth in the lung.

Conclusions

These data demonstrate that TRG is a smart material not only for treating primary tumors, but also for preventing metastasis and recurrence.

Introduction

Combination therapy for cancer treatment has shown promising outcomes such as prevention of recurrence and metastasis [1 2]. To elicit effective treatment against cancer, chemotherapy, immunotherapy, radiation therapy, gene therapy, photodynamic therapy, and photothermal therapy (PTT) have previously

been combined [3 4]. Various nanostructures and carriers have been studied for the combination of these therapies for cancer treatment [5 6]. Among them, hydrogels have shown positive results; for example, they exert low cytotoxic effects on the body, are biodegradable, and facilitate simple and easy incorporation of therapeutic materials [7 8].

Cancer therapy using PTT has recently received extensive attention, as it can induce a therapeutic effect by increasing temperature exclusively in the laser-irradiated area [5]. Generation of thermal energy from near-infrared (NIR) light requires an NIR absorber [9]. Delivery of the NIR absorber to tumor cells is the first step in PTT for cancer [10]. Targeted delivery of the absorber using carriers induces NIR irradiation-mediated apoptosis (programmed cell death) of specific cancer cells, thus reducing damage to healthy tissues [11]. Indocyanine green (ICG) is a NIR absorber that has been approved as an imaging agent for human use by the United States Food and Drug Administration and the European Medicine Agency [12 13]. In addition to its function as an imaging agent, ICG exerts a thermal responsive effect against NIR laser irradiation, which is frequently used in PTT [5]. However, ICG is limited in its use as a photosensitizer owing to its fast degradation and poor stability in the body [14]. Therefore, various nanomaterials have been evaluated for their efficacy in overcoming the limitations of ICG [15 16].

Immunotherapy against cancer involves activation of T-lymphocytes [17]. Antigen-specific cytotoxic T lymphocytes and helper T cells selectively kill antigen-expressing cancer cells, eliminating cancer metastasis and recurrence [18]. The activation of antigen-specific T-cells is mediated by antigen-presenting cells such as dendritic cells (DCs) and macrophages [19]. After stimulation by antigens, DCs upregulate co-stimulators and present antigens on the major histocompatibility complex (MHC) [20]. In addition, activated DCs secrete pro-inflammatory cytokines that induce T cell differentiation and activation. However, the antigens generated by cancer cells can neither promote sufficient activation of DCs nor promote their presentation because they are non-immunogenic antigens [20]. Cancer cell apoptosis also produces cancer antigens that do not fully activate DCs [21]. Therefore, for effective immunotherapy against cancer, immune stimulatory molecules and adjuvants are commonly included in therapeutic trials [22].

In murine, conventional DCs (cDCs) contain two subsets: cDC1 and cDC2. cDC1 presents intracellular antigen to CD8 T cells by MHC class I, while cDC2 promotes CD4 T cell activation by presentation of extracellular antigen on MHC class II [23]. Although both CD4 and CD8 T cell activation is required for cancer immunotherapy, anti-cancer immunity has been contributed by activated CD8 T cells, which are called cytotoxic T lymphocytes (CTLs) [24]. Antigen-specific CTL activation elicits selective killing of cancer cells based on the cancer cell-expressing antigen. Therefore, the induction of antigen-specific CTL activation is a desirable strategy for cancer immunotherapy [19].

Various types of hydrogels have been developed for cancer therapy, including injectable and attachable types [10 25]. Hydrogels have great advantages as carriers and can easily deliver anti-cancer drugs,

photosensitizers, and immune stimulators [7 26]. Owing to their excellent biocompatibility and biodegradability, polysaccharide-based hydrogels have been used to control drug delivery for the treatment of tumors [27 28]. Among the various types of polysaccharides, alginate (a natural biopolymer), has been used frequently for the synthesis of hydrogels because of its minimal toxicity, good biocompatibility, and biodegradability [29 30]. Moreover, collagen is an abundant protein in animals and a major component of connective tissues, which forms a triple helix structure [31 32]. The cross-linking of the molecular structure of collagen biopolymers with alginate, oxazolidine, or hyaluronic acid can increase their mechanical strength [31–33]. In this study, we fabricated a thermally responsive hydrogel (TRG) using sodium alginate cross-linked collagen and incorporated ICG as the photosensitizer. Moreover, TRG was incorporated with polyinosinic:polycytidylic acid (poly I:C), named pTRG, to elicit immune activation. We evaluated whether pTRG could eliminate the tumor by PTT and further prevent recurrence or metastasis of the cancer by cancer antigen-specific immunity.

Materials And Methods

Preparation of pTRG

Sodium alginate (Sigma Aldrich, St. Louis, MO, USA) was dissolved in deionized water (DW) to obtain a concentration of 40 mg/mL. Collagen (from calf skin, Sigma Aldrich) was dissolved in 0.1 M acetic acid to attain a concentration of 60 mg/mL. To trigger collagen fabrication, the solution was incubated at 37°C for 4 h. To prepare TRG, ICG (Tokyo Chemical Industry Co., Ltd., Tokyo, Japan), along with a 5% weight ratio of collagen, was dissolved in DW and added to the solution. pTRG was prepared using the same methods; except that the mixture of ICG and poly was I:C (0.8 mg/mL, HMW; InvivoGen, San Diego, CA), instead of ICG only. The pre-gel solution was treated with 150 mM $CaCl_2$ (Sigma-Aldrich). The difference between the gel and TRG preparation methods was the absence of ICG. For evaluation of the carrier effect of TRGs, the TRG was incorporated with phosphate buffered saline (PBS), 0.8 mg/mL of poly I:C (HMW, InvivoGen), 1.8 mg/mL of stimulator of interferon genes (STING) ligand (2'3'-cGAMP, InvivoGen), 6.3 mg/mL of anti-programmed cell death-1(PD-1) Ab (29F.1A, Bioxcell, Lebanon, NH, USA), or 4.4 mg/mL of anti-programmed cell death-ligand 1 (PD-L1) Ab (29F1A12, Bioxcell), respectively.

Characterization of pTRG

Scanning electron microscopy (SEM) images were obtained using an S-4800 scanning electron microscope (HITACHI, Japan) at the Core Research Support Center for Natural Products and Medical Materials at Yeungnam University, Republic of Korea. The absorption spectra and released poly I:C concentrations were measured using a UV/vis spectrophotometer (Cary 100 Bio, Varian Inc., USA). A fiber-coupled continuous-wave diode laser (808 nm, 10 W) was obtained from Changchun New Industries Optoelectronic Technology Co., Ltd. (China). Thermographic images of the temperature were obtained using the FLIR One Thermal Imaging System (FLIR Systems, Wilsonville, OR, USA).

Cell lines

The murine colon carcinoma cell line CT-26-iRFP (CT26.WT-iRFP-Neo; Imanis Life Sciences, CL091, Rochester, USA) was cultured in DMEM (Thermo Fisher Scientific, Inc., Waltham, MA, USA) supplemented with 10% fetal bovine serum (FBS, Sigma Aldrich), 1× penicillin/streptomycin (Gibco BRL Ltd, Paisley, Scotland), and 0.4 mg/mL G418 (Thermo Fisher Scientific, Inc.). The murine breast cancer cell line 4T1-iRFP (4T1.WT-iRFP-Neo; Imanis Life Sciences, CL078) were cultured in RPMI (Thermo Fisher Scientific, Inc.), supplemented with 10% FBS (Sigma Aldrich), 1× penicillin/streptomycin (Gibco BRL Ltd, Paisley, Scotland), 0.1 mg/mL G418 (Thermo Fisher Scientific, Inc.), and 2 μg/mL puromycin (InvivoGen). The cell lines were grown at 37°C in a humidified atmosphere containing 5% CO_2 and air.

Mice

BALB/c mice (6–8 weeks old, female) were obtained from Hyochang Science (Daegu, Republic of Korea). The mice were kept under pathogen-free conditions at the Laboratory Animals Center of Yeungnam University. All experiments were conducted after considering the basic ethical principles of animal experiments and the 3R principles. In addition, the experiment was conducted in compliance with the animal protection law, the law on experimental animals, and the IACUC regulations of Yeungnam University. The Committee on the Ethics of Animal Experiments of Yeungnam University Laboratory Animals Center approved the protocol (mouse protocol number, 2020-039). For ethical reasons, we minimized pain or stress in the animals by euthanizing them with CO_2 gas, in accordance with the humanitarian endpoint criteria.

First tumor challenge and PTT

BALB/c mice were subcutaneously injected with 1×10^6 CT-26-iRFP or 4T1-iRFP cells. After 7 days, the mice were randomly separated into six groups: PBS, poly I:C, Gel, pGel, TRG, and pTRG. After intratumorally (*i.t.*) injection of each sample into the mice, the tumor was irradiated with an NIR laser at 1.5 W/cm^2 for 5 min. The elevated temperature was imaged using the FLIR One Thermal Imaging System (FLIR Systems). The tumor volume was monitored on day 28 after tumor challenge and calculated using the formula V = ½ (length × width^2).

Antibodies

Anti-IgG1 antibody (Ab), anti-IgG2a Ab, and anti-IgG2b Ab were used as isotype controls and purchased from BioLegend (San Diego, CA, USA). Anti-TCR-β (H57-597), anti-CD4 (GK1.5), anti-CD8α (53 − 6.7), anti-interferon (IFN-γ (B27), anti-CD11c (N418), anti-CD40 (HM40-3), anti-CD80 (16-10A1), anti-CD86 (GL-1), anti-MHC class I (AF6-88.5), and anti-MHC class II (M5/114.15.2) were purchased from BioLegend.

Mouse lymphoid DC analysis

Tumor-draining lymph nodes (tdLNs) were homogenized using a slide class. Lipids and debris were removed though 100 nm nylon mash. After washing with PBS, the cells were stained with fluorescence-labeled Abs for 30 min. To define DCs, the cells were stained with lineage markers, including anti-B220 (RA3-6B2), anti-CD3 (17A2), anti-CD49b (DX5), anti-Gr1 (RB68C5), anti-Thy1.1 (OX-7), and anti-TER-119 (TER-119). Lineage$^-$CD11c$^+$ cells were further divided into cDC1 and cDC2 cells. Co-stimulator and MHC

molecule levels were measured in cDC1 and cDC2 using a NovoCyte flow cytometer (ACEA Biosciences Inc., San Diego, CA, USA).

Flow cytometry analysis

The tdLN cells were stained with unlabelled isotype control Abs and Fc-block Abs (BioLegend) for 15 min to prevent non-specific binding of Abs. After washing with PBS, the cells were stained with fluorescence-conjugated antibodies at 4°C for 30 min. After removing free Abs by washing with PBS, the cells were suspended with 4',6-diamidino-2-phenylindole (Sigma Aldrich) containing flow cytometry buffer (BioLegend) and were analyzed using a NovoCyte flow cytometer (ACEA Biosciences Inc.).

Second tumor challenge

The cured mice from the first challenge of CT-26 or 4T1 were injected intravenously with CT-26-iRFP cells (0.7×10^6/100 μL of PBS) or 4T1-iRFP (0.5×10^6/100 μL of PBS), respectively. On day 10 after the second cancer challenge, the mice were sacrificed, and their lungs and spleen were harvested for further experiments.

In vivo **fluorescence imaging**

iRFP fluorescence images were captured using the fluorescence *in vivo* imaging system, FOBI (Cellgentek, Cheongju, Republic of Korea) on the first and second challenges.

Histology

As previously described in detail, lung samples were harvested 10 days after the second tumor challenge and fixed with 10% formalin. After rehydration by gradient change of ethanol, the lungs were embedded in paraffin. The lung tissue was sectioned to a thickness of 5 μm using a microtome and attached to a glass slide. The sections were rehydrated and stained with hematoxylin and eosin. Tumor infiltration in the lung was observed using an EVOS M5000 microscope (Invitrogen, Waltham, MA, USA).

Analysis of CT-26 specific T cell immunity

CT-26 cells (1×10^7 CT-26 cells were freeze-dried and thawed three times to obtain a lysate. After centrifugation (10,000 × *g*, at 4°C for 5 min), the concentration of CT-26 lysate was determined in the supernatant using the Bradford assay. Splenocytes (1×10^6 splenocytes) were treated with 10 μg/mL CT-26 cell lysates. Twenty-four hours after incubation, the cells were stained with surface antibodies (APC/Cy7-anti-TCR-β, PerCP5.5-anti-CD4, and BV785-anti-CD8α) for 20 min. After washing with PBS, the cells were fixed and permeabilized with intracellular staining buffer (BioLegend) at 4°C for 30 min. After washing, the cells were incubated with intracellular antibodies (PE-anti-IFN-γ) for 30 min. IFN-γ-producing CD4 and CD8 T cells were analyzed using NovoCyte (ACEA Biosciences Inc.).

Enzyme-linked immunosorbent assay (ELISA)

Serum concentrations of interleukin (IL)-6, IL-12p70, and tumor necrosis factor (TNF)-α were measured 24 h after the first tumor therapy using ELISA kits (BioLegend). The antigen-specific production of TNF-α,

IFN-γ, perforin, and granzyme B in cultured medium was analyzed 24 h after stimulation of splenocytes with 10 μg/mL of CT-26 lysate.

In vivo **cytotoxicity assay**

Splenocytes were harvested from BLAB/c mice and labeled with 200 nM of CFSE or 10 mM CellTracker™ Orange CMTMR (Life Technologies). The CFSE-labeled splenocytes were coated with 200 nM of CT-26 antigen AH1 (SPSYVYHQF) peptide and the CMTMR-labeled cells were loaded with the control peptide. The CFSE and CMTMR-labeled cells were mixed at a 1:1 ratio, and a total of 10×10^6 labeled cells were transferred to BLAB/c mice, which were treated with TRG and pTRG for the first time. The PBS, poly I:C, and pGel-treated mice were also transferred to labeled cells as controls. Twelve hours after splenocyte transfer, the spleen was harvested, and specific killing was analyzed using NovoCyte (ACEA Biosciences Inc.).

Depletion of CD4 and CD8 cells

After treatment of the first tumor by PTT, the cured mice received 1 mg/kg of anti-CD4 Ab (GK1.5, 1) or 1 mg/kg of anti-CD8 Ab (YTS169.4) (both from BioXcell) every 2 days from 28 days after the 1st tumor challenge (2 days before the 2nd challenge of cancer cells). The depletion efficacy of Ab injection was analyzed using NovoCyte (ACEA Biosciences Inc.) and showed > 98% depletion of CD4 or CD8 cells in the mice.

Statistical analysis

The data were analyzed using SPSS (Chicago, IL, USA) and expressed as the mean ± standard error of the mean. The values *$p < 0.05$*, and **$p < 0.01$* were considered statistically significant.

Results

Preparation and characterization of TRG

Sodium alginate-cross-linked collagen was mixed with $CaCl_2$ to form a hydrogel at 37°C. At 60°C, the gel changed into a fluid (Fig. 1A). As the gel was co-assembled with alginate and collagen, the SEM image showed a cross-section with a typical microporous composition (Fig. 1B). Owing to its microporous composition, the gel retained ICG and was thus called a TRG. TRG was further incorporated into poly I:C (pTRG). As shown in Fig. 1C, TRG and pTRG showed maximum absorbance at 780 nm. For the evaluation of photothermal efficiency, TRG and pTRG were irradiated with an NIR laser (1.5 W/cm^2 for 5 min), which resulted in an efficient increase in the temperature to over 60°C (Fig. 1D), and the gel changed to fluid at 60°C. Next, we examined whether poly I:C was released from pTRG by NIR irradiation. Poly I:C (0.556 ± 0.02 mg/mL was released from pTRG after 5 min of NIR laser irradiation, whereas poly I:C-containing Gel (pGel, without ICG did not release poly I:C (Fig. 1E). To determine the stability of pTRG in an aqueous solution, it was kept in an FBS-containing culture medium at different temperatures for 7 days. The cumulative poly I:C released from pTRG was 0.79 ± 0.01, 0.16 ± 0.05, and 0.04 ± 0.005 mg/mL

at 60°C, 37°C, and 4°C, respectively (Fig. 1F). Thus, these results indicated that pTRG functions as a photothermal material when exposed to an NIR laser.

Evaluation of photothermal therapeutic effect of TRG and pTRG against CT-26 tumor

Based on the thermal responsive effect of the hydrogel, we evaluated its photothermal therapeutic effect against CT-26 carcinoma in BALB/c mice. CT-26 tumor-bearing mice were *i.t.* injected with the hydrogels 7 days after the tumor injection. Under irradiation of NIR laser (1.5 W/cm^2) for 5 min, the temperatures of the TRG- and pTRG-injected tumors were greatly increased, with the maximum temperature of TRG and pTRG being 63.3 ℃ (± 0.49 ℃) and 62.7 ℃ (± 0.94 ℃), respectively (Fig. 2A). The temperature of PBS-, poly I:C only, Gel-, or pGel-treated tumors did not change considerably under NIR laser irradiation (Fig. 2A). As shown in the fluorescence images of tumors in Fig. 2B, TRG and pTRG treatment with laser irradiation eliminated tumor mass in the mice, while other controls detected large tumor masses in the mice. Additionally, the laser-irradiated mice tumors that received TRG and pTRG showed dramatic decreases in the size of the tumor mass and the remaining burn wound on day 15 after tumor injection, which completely disappeared on day 24 after tumor injection (Fig. 2C). As shown in the tumor growth curve in Fig. 2D, TRG and pTRG with laser irradiation completely diminished CT-26 tumor growth, while the tumor volumes were gradually increased in the other controls. Consequently, the TRG and pTRG with NIR laser-irradiated mice survived the CT-26 tumor challenge, while other control-treated mice died within 27 days after CT-26 tumor injection (Fig. 2E). Therefore, these data suggest that TRG and pTRG effectively eliminate CT-26 tumor growth by PTT.

DCs in tdLNs were activated by pTRG and NIR laser irradiation

As increased temperatures promote the release of poly I:C from the gel, we examined whether the released poly I:C induced the activation of DCs in tdLNs (Fig. 3A). CT-26 tumor-bearing mice were treated with hydrogels and irradiated with an NIR laser. Consistent with Fig. 2A, the temperatures were elevated in TRG-and pTRG-treated tumors (Figure S1). Twenty-four hours after NIR irradiation, the tdLNs were harvested and the cDC subsets in tdLN cells were defined as shown in Fig. 3B. The pTRG and NIR laser irradiation induced dramatic upregulation of CD40, 80, 86, MHC class I and II expression in both cDC1 and cCD2, which was almost similar to the poly I:C treatment alone (Fig. 3C). In addition, the serum concentrations of IL-6, IL-12p70, and TNF-α were substantially increased by pTRG treatment with laser irradiation (Fig. 3D). In contrast with the pTRG treatment, Gel, pGel, and TRG treatment with laser irradiation did not elicit activation of DC and cytokine production (Fig. 3C and D). Therefore, these data suggest that pTRG and laser irradiation can induce the activation of DCs in tdLNs.

Prevention of second challenge CT-26 tumor growth in the pTRG-mediated cured mice

Next, we examined the preventive effect of pTRG against the second tumor challenge. The mice cured from the first challenge of CT-26 by TRG and pTRG treatment were challenged again with CT-26 cells via intravenous injection. In addition, PBS-, poly I:C-, and pGel-treated mice, which did not challenge the first tumor, were injected intravenously with CT-26 cells as controls. As shown in Fig. 4A, PBS, poly I:C, and pGel-treated mice died within 13 days of tumor injection. Although the cured mice from the first injection of CT-26 by TRG delayed the death of the mice, the mice died within 20 days of the second CT-26 challenge (Fig. 4A). On the other hand, pTRG-mediated cured mice from the first CT-26 challenge survived until day 26 after the second CT-26 challenge (Fig. 4A). Moreover, metastatic CT-26 tumor growth was remarkably increased in the lung on day 10 after the second tumor challenge that was treated with PBS, poly I:C, or pGel (Fig. 4B and C). Notably, pTRG completely prevented second challenge-induced cancer growth in the lungs of mice cured from the first CT-26 challenge, whereas mice cured by TRG showed CT-26 tumor cell infiltration in the lung (Fig. 4B and C). In the histological data, the infiltration of CT-26 tumor cells in the lung was completely inhibited by pTRG-treated first tumor-cured mice, whereas the cured mice from the first tumor challenge by TRG did not successfully prevent second challenge CT-26 cell infiltration in the lung (Fig. 4D). Therefore, these data suggest that pTRG-mediated first tumor therapy could prevent metastasis and recurrence of the tumor.

pTRG induced antigen-specific T cell immunity

pTRG-mediated PTT induced apoptosis of CT-26, which produces the CT-26 antigen. In addition, released poly I:C from pTRG promoted the activation of DCs in tdLNs. Furthermore, pTRG-treated mice prevented the second tumor growth. Thus, these data prompted us to examine whether pTRG treatment can elicit CT-26 antigen-specific T cell immunity and whether T cells have an anti-cancer effect against the second challenge of CT-26. On day 10 after the second tumor challenge, the splenocytes were harvested and stimulated with CT-26 lysate and showed that intracellular production of IFN-γ in CD4 and CD8 T cells was greatly increased in pTRG-treated mice (Fig. 5A and B). However, CD4 and CD8 T cells in the first tumor-cured mice by TRG and other controls did not produce IFN-γ in response to the CT-26 lysate (Fig. 5A and B). In addition, the concentrations of TNF-α, IFN-γ, perforin, and granzyme B were significantly increased in the pTRG-treated splenocytes by CT-26 lysate compared to the other treatments (Fig. 5C). More importantly, pTRG-treated cured mice from the first challenge of CT-26 elicited specific killing of CT-26 antigen-coated splenocytes (Fig. 5D). Further evaluation of CD4 and CD8 T cell contribution in the prevention of second challenge CT-26 growth showed that the mice cured with pTRG were depleted of CD4 and CD8 cells; and found that CD4 and CD8 depleted mice failed to prevent against second challenged CT-26 growth in the lungs (Fig. 5E). Thus, these data suggest that pTRG-induced first transplanted tumor therapy promotes cancer antigen-specific T cell immunity, which mainly contributes to the prevention of the second challenge in tumor growth in mice.

Preventive effect of secondary challenge 4T1 tumor growth through pTRG

Next, we examined whether pTRG can treat 4T1 tumors, a candidate tumor model for PTT, and the most well-defined metastatic cancer in the murine model. The 4T1 tumor-bearing BLAB/c mice were *i.t.* injected

with PBS, poly I:C, Gel, pGel, TRG, and pTRG irradiated with NIR laser (Figure S2). In mice treated with TRG and pTRG under NIR laser irradiation, the first challenged 4T1 tumor was eliminated, whereas the other control treatment failed to eliminate the tumor (Fig. 6A). Furthermore, the second challenge of 4T1 cells to mice treated with pTRG completely blocked the infiltration of 4T1 cancer cells into the lung, whereas TRG-mediated cured mice from the first challenge failed to protect 4T1 cell infiltration of the lung (Fig. 6B, C, and D). Therefore, these data suggest that pTRG can be used for the treatment of breast cancer by PTT, and it can prevent metastasis by immunotherapy.

Cancer therapeutic carrier effect of TRG for immunotherapy

Since TRG can incorporate several types of molecules, we further examined whether TRG can act as a cancer therapeutic carrier for the delivery of immunotherapeutic molecules. To evaluate TRG as a cancer therapeutic carrier, TRG was incorporated with poly I:C, of stimulator of interferon genes (STING) ligand, anti-PD-1 Abs, and anti-PD-L1 Abs. CT-26 tumor-bearing mice were *i.t.* injected with TRG comprising poly I:C, STING ligand, anti-PD-1 Ab, or anti-PD-L1 Ab and irradiated with NIR laser (Figure S3). Twenty days after the primary tumor injection, mice treated with immunotherapeutic molecules containing TRGs completely eliminated the first challenged tumor (Fig. 7A). The cured mice from the first challenge of CT-26 were rechallenged with CT-26 cells by intravenous injection and showed that TRGs containing poly I:C, STING ligand, anti-PD-1 Ab, or anti-PD-L1 Ab effectively eradicated CT-26 cancer infiltration in the lungs (Fig. 7B and C). Therefore, these data revealed that TRG can be used as a carrier of cancer therapeutic molecules, especially immunotherapeutic reagents.

Discussion

The advantage of hydrogels is that they can contain many kinds of substances [34]. In this study, we introduced ICG into the hydrogel to induce a thermal response using an NIR laser. Moreover, we induced the release of poly I:C from the hydrogel, as high temperatures promoted the melting of the hydrogel [35]. In mice in an *in vivo* setting, intramural injection of pTRG and NIR laser irradiation promoted apoptotic and necrotic cell death in CT-26 tumors and may have produced apoptotic bodies and tumor antigens [20 36]. In addition to apoptosis and necrosis of CT-26 cells by PTT, incorporated poly I:C was released from the pTRG. Therefore, poly I:C together with CT-26 associated antigen-stimulated DCs elicited CT-26 antigen-specific T cell immunity. Consequently, these immune responses prevented the second challenge of CT-26 cancer growth in the lungs.

In the past, surgery, chemotherapy, and radiotherapy were the most common treatment methods for cancer [37]. However, these treatments are limited to metastatic cancer [2]. Moreover, surgical tumor treatment cannot effectively prevent tumor recurrence [38]. Since immunotherapy has been established, various treatments have been combined to prevent metastasis and recurrence of cancer [39]. In this study, we designed a combination therapy that treated the first transplanted tumor with PTT and prevented second-challenge lung metastatic cancer growth by immunotherapy. The PTT-mediated cell death

produced cancer antigen, and the release of poly I:C in the TRG may promote cancer antigen-specific immune activation, which consequently prevents the second challenge of tumor growth in the lung.

PTT induces immunogenic cell death, which stimulates immune cells via damage-associated molecular patterns (DAMPs) [40]. Immunogenic cell death is accompanied by the release of numerous DAMPs from dying cancer cells, which stimulate and recruit antigen-presenting cells [41]. Although a number of studies have shown that immunogenic cell death can effectively treat tumors by immune activity, there has not been an active study on the prevention of recurrence and metastatic cancer growth [21 40]. In this study, we found that TRG-mediated cured mice from the first challenge with CT-26 also suppressed the second challenge in tumor growth in the lungs. However, the prevention effect in these mice was not sufficient to eliminate tumor growth caused by the second challenge, as shown in Fig. 4. Our previous study also showed that the cured mice from the first tumor inoculated with PTT only partially inhibited the second challenge in tumor growth, and the mice eventually died due to cancer growth [20]. These data indicate that anti-cancer immunity induced by immunogenic cell death is not sufficient to prevent recurrence or metastatic cancer growth. Since DAMPs secreted from immunogenic cell death are cancer cell-derived substances, we added an immune stimulator to elicit cancer antigen-specific immune activity. This prevented the second challenge of cancer growth in the lungs. Therefore, these data suggest that the combination of cancer cell-associated DAMPs and immune stimulators can elicit anti-cancer immunity.

Cancer treatment using hydrogels is being attempted because they can effectively supply drugs. In a recent study, immunostimulatory molecules or immune checkpoint inhibitors were incorporated into hydrogels and showed preventive effects against metastatic cancer [42–45]. However, when applying the hydrogel, the first transplanted tumor was surgically removed, and the hydrogel was attached to the surgical site, which effectively prevented second-challenged metastatic cancer growth [42]. However, it is difficult to apply this method to actual patients because only 90% of the tumors were surgically removed in order to induce the expression of cancer antigens [42]. In this study, a method of killing primary cancers in the body was applied to induce the expression of cancer antigens. Hydrogel-mediated PTT was applied to the first challenged tumor to induce the expression of cancer antigens. As can be seen from the results, besides the purpose of antigen release, it showed perfect treatment efficacy against the first challenged tumor. In addition, the immunotherapeutic substance contained in TRG was effectively secreted and induced antigen-specific immune activity, which completely blocked secondary-challenged metastatic cancer. Therefore, the TRG developed in this study will be more efficient and effective for cancer treatment than the hydrogels used in previous studies.

In this study, we synthesized an injectable hydrogel that responds to an NIR laser to increase the temperature and secrete the incorporated molecules. By the pTRG, the first challenged tumor was eliminated by PTT, and the second challenge of lung metastatic cancer was prevented by immunotherapy. In addition, TRG can carry various immunotherapeutic molecules and can effectively treat cancer. Thus, these data suggest that pTRG, which can be used as a carrier of immunotherapeutic

reagents, is a smart material that can not only treat primary tumors but can also prevent metastatic or recurrent cancer.

Abbreviations

PTT, photothermal therapy; NIR, near-infrared; ICG, indocyanine green; DCs, dendritic cells; MHC, major histocompatibility complex; cDCs, conventional DCs; CTLs, cytotoxic T lymphocytes; TRG, thermally responsive hydrogel; poly I:C, polyinosinic:polycytidylic acid; DW, deionized water; STING, stimulator of interferon genes; PD-1, programmed cell death-1; PD-L1, programmed cell death-ligand 1; PBS, phosphate buffered saline; SEM, scanning electron microscopy; FBS, fetal bovine serum; *i.t.*; intratumorally; Ab; antibody; IFN, interferon; tdLNs, tumor-draining lymph nodes; ELISA, Enzyme-linked immunosorbent assay; IL, interleukin; TNF, tumor necrosis factor DAMPs, damage-associated molecular patterns

Declarations

Ethics approval

The animal protocol, 2020-039, was approved by the Committee on the Ethics of Animal Experiments at the Yeungnam University Animal Facility. This study was conducted in accordance with the guidelines of the Institutional Animal Care and Use Committee at the Yeungnam University Animal Facility.

Availability of data and material

All data relevant to the study are included in the article or uploaded as online supplemental information.

Competing interests

None declared.

Funding

This study was supported by the National Research Foundation of Korea [NRF-2019R1C1C1003334 and NRF-2020R1A6A1A03044512].

Author’s contributors

J.H. and J.O.J. conceived and designed the experiments. J.H., E.K.A., and W.Z. performed the experiments. J.H. and E.K.A. analyzed the data. J.O.J. supervised the project. J.H. and J.O.J. wrote the manuscript. W.Z. and J.O.J. discussed the results and commented on the manuscript.

Acknowledgments

We thank the Yeungnam University animal facility for maintaining the animals used in this study and the Core Research Support Center for Natural Products and Medical Materials (CRCNM) for their technical

support.

References

1. Nam J, Son S, Ochyl LJ, et al. Chemo-photothermal therapy combination elicits anti-tumor immunity against advanced metastatic cancer. Nat Commun 2018;9(1):1074. doi: 10.1038/s41467-018-03473-9 [published Online First: 2018/03/16]
2. Peitzsch C, Tyutyunnykova A, Pantel K, et al. Cancer stem cells: The root of tumor recurrence and metastases. Semin Cancer Biol 2017;44:10–24. doi: 10.1016/j.semcancer.2017.02.011 [published Online First: 2017/03/05]
3. Asna N, Livoff A, Batash R, et al. Radiation therapy and immunotherapy-a potential combination in cancer treatment. Curr Oncol 2018;25(5):e454-e60. doi: 10.3747/co.25.4002 [published Online First: 2018/11/23]
4. Jin JO, Kim G, Hwang J, et al. Nucleic acid nanotechnology for cancer treatment. Biochim Biophys Acta Rev Cancer 2020;1874(1):188377. doi: 10.1016/j.bbcan.2020.188377 [published Online First: 2020/05/19]
5. Han HS, Choi KY. Advances in Nanomaterial-Mediated Photothermal Cancer Therapies: Toward Clinical Applications. Biomedicines 2021;9(3) doi: 10.3390/biomedicines9030305 [published Online First: 2021/04/04]
6. Thorat ND, Bauer J. Functional smart hybrid nanostructures based nanotheranostic approach for advanced cancer treatment. Applied Surface Science 2020;527:146809.
7. Cirillo G, Spizzirri UG, Curcio M, et al. Injectable Hydrogels for Cancer Therapy over the Last Decade. Pharmaceutics 2019;11(9) doi: 10.3390/pharmaceutics11090486 [published Online First: 2019/09/25]
8. Trombino S, Servidio C, Curcio F, et al. Strategies for Hyaluronic Acid-Based Hydrogel Design in Drug Delivery. Pharmaceutics 2019;11(8) doi: 10.3390/pharmaceutics11080407 [published Online First: 2019/08/15]
9. Kim HS, Lee DY. Near-Infrared-Responsive Cancer Photothermal and Photodynamic Therapy Using Gold Nanoparticles. Polymers (Basel) 2018;10(9) doi: 10.3390/polym10090961 [published Online First: 2019/04/10]
10. Hwang J, Jin JO. Attachable Hydrogel Containing Indocyanine Green for Selective Photothermal Therapy against Melanoma. Biomolecules 2020;10(8) doi: 10.3390/biom10081124 [published Online First: 2020/08/06]
11. Mitsunaga M, Ogawa M, Kosaka N, et al. Cancer cell-selective in vivo near infrared photoimmunotherapy targeting specific membrane molecules. Nat Med 2011;17(12):1685–91. doi: 10.1038/nm.2554 [published Online First: 2011/11/08]
12. Mordon S, Devoisselle JM, Soulie-Begu S, et al. Indocyanine green: physicochemical factors affecting its fluorescencein vivo. Microvascular research 1998;55(2):146–52.

13. Ishizawa T, Masuda K, Urano Y, et al. Mechanistic background and clinical applications of indocyanine green fluorescence imaging of hepatocellular carcinoma. Annals of surgical oncology 2014;21(2):440–48.
14. Saxena V, Sadoqi M, Shao J. Degradation kinetics of indocyanine green in aqueous solution. J Pharm Sci 2003;92(10):2090–7. doi: 10.1002/jps.10470 [published Online First: 2003/09/23]
15. Park T, Lee S, Amatya R, et al. ICG-Loaded PEGylated BSA-Silver Nanoparticles for Effective Photothermal Cancer Therapy. Int J Nanomedicine 2020;15:5459–71. doi: 10.2147/IJN.S255874 [published Online First: 2020/08/18]
16. Saboktakin M. Polymeric Nanoencapsulation of Indocyanine green for Photodynamic Therapy Technique. J Biomed Res Rev 2019;2:62–76.
17. Waldman AD, Fritz JM, Lenardo MJ. A guide to cancer immunotherapy: from T cell basic science to clinical practice. Nat Rev Immunol 2020;20(11):651–68. doi: 10.1038/s41577-020-0306-5 [published Online First: 2020/05/21]
18. Gonzalez H, Hagerling C, Werb Z. Roles of the immune system in cancer: from tumor initiation to metastatic progression. Genes Dev 2018;32(19–20):1267–84. doi: 10.1101/gad.314617.118 [published Online First: 2018/10/03]
19. Zhang W, Xu L, Park HB, et al. Escherichia coli adhesion portion FimH functions as an adjuvant for cancer immunotherapy. Nat Commun 2020;11(1):1187. doi: 10.1038/s41467-020-15030-4 [published Online First: 2020/03/07]
20. Xu L, Zhang W, Park HB, et al. Indocyanine green and poly I:C containing thermo-responsive liposomes used in immune-photothermal therapy prevent cancer growth and metastasis. J Immunother Cancer 2019;7(1):220. doi: 10.1186/s40425-019-0702-1 [published Online First: 2019/08/16]
21. Lamberti MJ, Nigro A, Mentucci FM, et al. Dendritic Cells and Immunogenic Cancer Cell Death: A Combination for Improving Antitumor Immunity. Pharmaceutics 2020;12(3) doi: 10.3390/pharmaceutics12030256 [published Online First: 2020/03/18]
22. Temizoz B, Kuroda E, Ishii KJ. Vaccine adjuvants as potential cancer immunotherapeutics. Int Immunol 2016;28(7):329–38. doi: 10.1093/intimm/dxw015 [published Online First: 2016/03/24]
23. Matsuo K, Yoshie O, Kitahata K, et al. Recent Progress in Dendritic Cell-Based Cancer Immunotherapy. Cancers (Basel) 2021;13(10) doi: 10.3390/cancers13102495 [published Online First: 2021/06/03]
24. Hwang J, Zhang W, Park HB, et al. Escherichia coli adhesin protein-conjugated thermal responsive hybrid nanoparticles for photothermal and immunotherapy against cancer and its metastasis. J Immunother Cancer 2021;9(7) doi: 10.1136/jitc-2021-002666 [published Online First: 2021/07/08]
25. Hyun H, Park MH, Jo G, et al. Injectable Glycol Chitosan Hydrogel Containing Folic Acid-Functionalized Cyclodextrin-Paclitaxel Complex for Breast Cancer Therapy. Nanomaterials (Basel) 2021;11(2) doi: 10.3390/nano11020317 [published Online First: 2021/01/31]
26. Komatsu S, Asoh T-A, Ishihara R, et al. Fabrication of thermoresponsive degradable hydrogel made by radical polymerization of 2-methylene-1, 3-dioxepane: Unique thermal coacervation in hydrogel.

Polymer 2019;179:121633.
27. Abasalizadeh F, Moghaddam SV, Alizadeh E, et al. Alginate-based hydrogels as drug delivery vehicles in cancer treatment and their applications in wound dressing and 3D bioprinting. J Biol Eng 2020;14:8. doi: 10.1186/s13036-020-0227-7 [published Online First: 2020/03/20]
28. Sood A, Gupta A, Agrawal G. Recent advances in polysaccharides based biomaterials for drug delivery and tissue engineering applications. Carbohydrate Polymer Technologies and Applications 2021;2:100067.
29. Lee KY, Mooney DJ. Alginate: properties and biomedical applications. Prog Polym Sci 2012;37(1):106–26. doi: 10.1016/j.progpolymsci.2011.06.003 [published Online First: 2011/11/30]
30. Pishavar E, Khosravi F, Naserifar M, et al. Multifunctional and Self-Healable Intelligent Hydrogels for Cancer Drug Delivery and Promoting Tissue Regeneration In Vivo. Polymers (Basel) 2021;13(16) doi: 10.3390/polym13162680 [published Online First: 2021/08/29]
31. Deepthi S, Nivedhitha Sundaram M, Deepti Kadavan J, et al. Layered chitosan-collagen hydrogel/aligned PLLA nanofiber construct for flexor tendon regeneration. Carbohydr Polym 2016;153:492–500. doi: 10.1016/j.carbpol.2016.07.124 [published Online First: 2016/08/27]
32. Kupper S, Klosowska-Chomiczewska I, Szumala P. Collagen and hyaluronic acid hydrogel in water-in-oil microemulsion delivery systems. Carbohydr Polym 2017;175:347–54. doi: 10.1016/j.carbpol.2017.08.010 [published Online First: 2017/09/18]
33. Lee SJ, Seok JM, Lee JH, et al. Three-Dimensional Printable Hydrogel Using a Hyaluronic Acid/Sodium Alginate Bio-Ink. Polymers (Basel) 2021;13(5) doi: 10.3390/polym13050794 [published Online First: 2021/04/04]
34. Zagorska-Dziok M, Sobczak M. Hydrogel-Based Active Substance Release Systems for Cosmetology and Dermatology Application: A Review. Pharmaceutics 2020;12(5) doi: 10.3390/pharmaceutics12050396 [published Online First: 2020/05/03]
35. Qing G, Zhao X, Gong N, et al. Thermo-responsive triple-function nanotransporter for efficient chemo-photothermal therapy of multidrug-resistant bacterial infection. Nat Commun 2019;10(1):4336. doi: 10.1038/s41467-019-12313-3 [published Online First: 2019/09/26]
36. Li W, Yang J, Luo L, et al. Targeting photodynamic and photothermal therapy to the endoplasmic reticulum enhances immunogenic cancer cell death. Nat Commun 2019;10(1):3349. doi: 10.1038/s41467-019-11269-8 [published Online First: 2019/07/28]
37. Baudelet M, Van den Steen L, Duprez F, et al. Study protocol for a randomized controlled trial: prophylactic swallowing exercises in head-and-neck cancer patients treated with (chemo)radiotherapy (PRESTO trial). Trials 2020;21(1):237. doi: 10.1186/s13063-020-4171-0 [published Online First: 2020/03/04]
38. Zou L, Wang H, He B, et al. Current Approaches of Photothermal Therapy in Treating Cancer Metastasis with Nanotherapeutics. Theranostics 2016;6(6):762–72. doi: 10.7150/thno.14988 [published Online First: 2016/05/11]

39. Edwards SC, Hoevenaar WHM, Coffelt SB. Emerging immunotherapies for metastasis. Br J Cancer 2021;124(1):37–48. doi: 10.1038/s41416-020-01160-5 [published Online First: 2020/12/03]
40. Li Y, Liu X, Pan W, et al. Photothermal therapy-induced immunogenic cell death based on natural melanin nanoparticles against breast cancer. Chem Commun (Camb) 2020;56(9):1389–92. doi: 10.1039/c9cc08447a [published Online First: 2020/01/09]
41. Alzeibak R, Mishchenko TA, Shilyagina NY, et al. Targeting immunogenic cancer cell death by photodynamic therapy: past, present and future. J Immunother Cancer 2021;9(1) doi: 10.1136/jitc-2020-001926 [published Online First: 2021/01/13]
42. Park CG, Hartl CA, Schmid D, et al. Extended release of perioperative immunotherapy prevents tumor recurrence and eliminates metastases. *Sci Transl Med* 2018;10(433) doi: 10.1126/scitranslmed.aar1916 [published Online First: 2018/03/23]
43. Ma H, He C, Chen X. Injectable Hydrogels as Local Depots at Tumor Sites for Antitumor Immunotherapy and Immune-Based Combination Therapy. Macromol Biosci 2021;21(6):e2100039. doi: 10.1002/mabi.202100039 [published Online First: 2021/04/06]
44. Leach DG, Young S, Hartgerink JD. Advances in immunotherapy delivery from implantable and injectable biomaterials. Acta Biomater 2019;88:15–31. doi: 10.1016/j.actbio.2019.02.016 [published Online First: 2019/02/17]
45. Huang X, Lu Y, Guo M, et al. Recent strategies for nano-based PTT combined with immunotherapy: from a biomaterial point of view. Theranostics 2021;11(15):7546–69. doi: 10.7150/thno.56482 [published Online First: 2021/06/24]

Figures

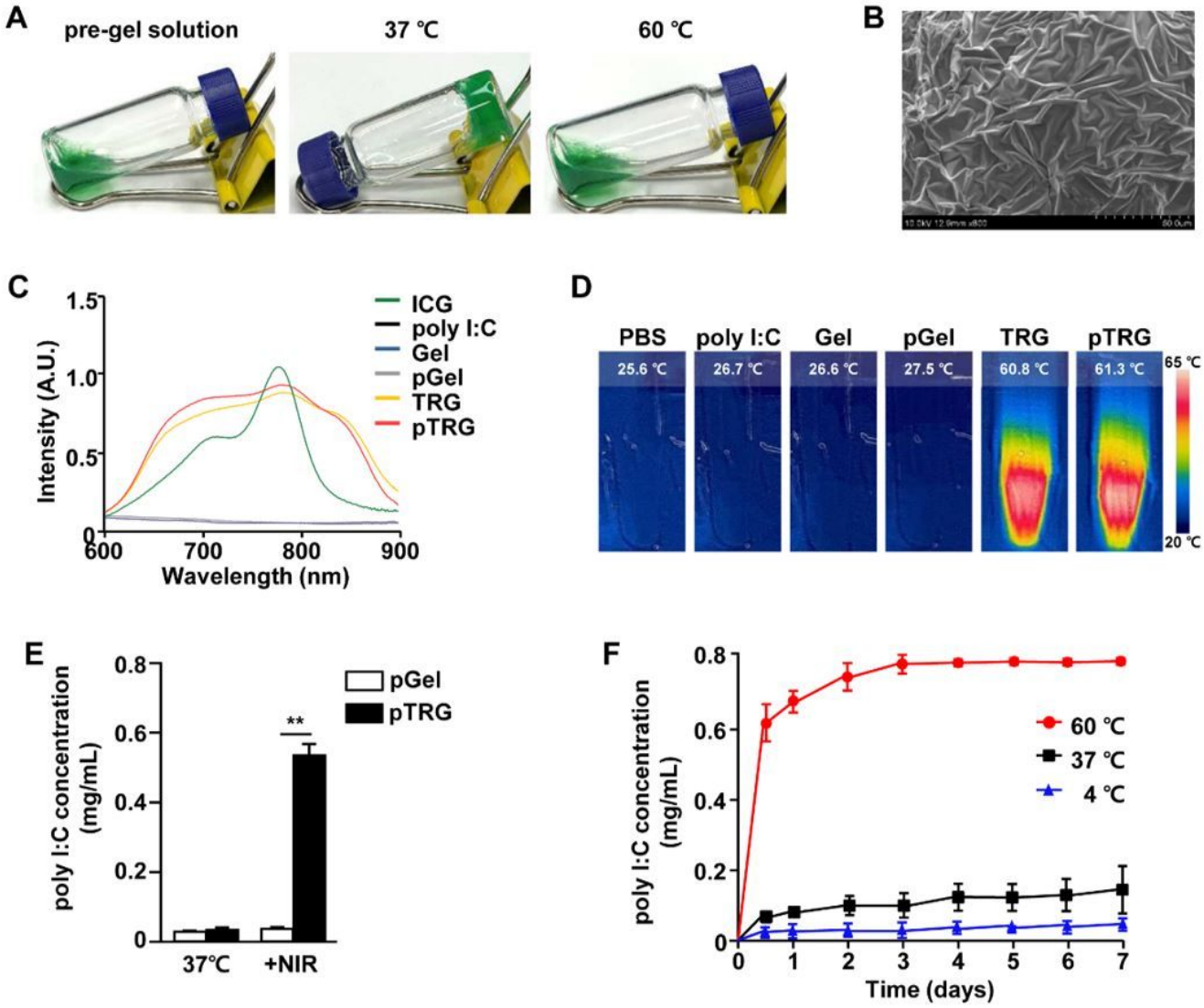

Figure 1

Characterization of thermal responsive hydrogel (TRG). (A) The photograph of TRG at different temperatures. (B) The scanning electron microscopy (SEM) image of the lyophilized TRG. (C) UV-vis NIR absorption spectra of free ICG, poly I:C, Gel, poly I:C-containing Gel (pGel), ICG-incorporated TRG and poly I:C-containing TRG (pTRG). (D) The thermographic images of PBS, poly I:C, Gel, pGel, TRG, and pTRG 5 min under NIR laser irradiation with a laser power density of 1.5 W/cm^2. (E) Poly I:C release from pGel and pTRG in PBS at the 37 °C or under NIR laser irradiation (1.5 W/cm^2, 5 min; ***p <0.01*). (F) Cumulative release of poly I:C from pGel after laser irradiation (1.5 W/cm^2, 5 min). The percentage of the poly I:C released was measured in the supernatant after the indicated time.

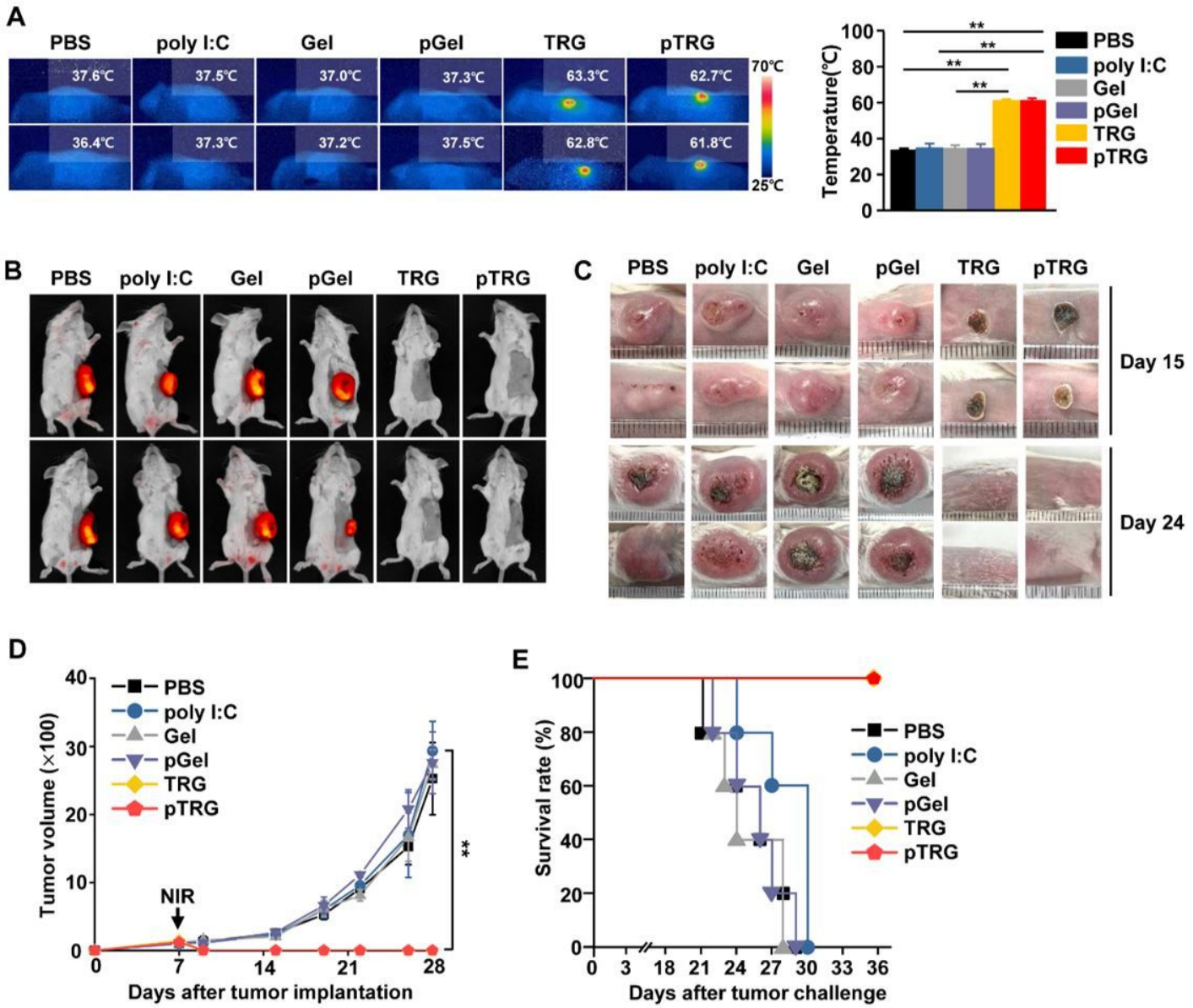

Figure 2

Photothermal therapy (PTT) through treatment of pTRG with NIR laser irradiation protected mice from CT-26 tumor. BALB/c mice were subcutaneously (*s.c.*) injected with 1×10^6 CT-26-iRFP cells. On day 7 of the tumor inoculation, the mice intratumorally (*i.t.*) received with PBS, poly I:C, Gel, pGel, TRG, and pTRG with NIR laser irradiation for 5 min with a laser power density of 1.5 W/cm^2. (A) The thermographic images of surface temperature on tumor site (left panel). The mean temperature after NIR laser irradiation (right panel, n=6 mice, two-way ANOVA, mean ± SEM, ***p <0.01*). (B) Fluorescence image of CT-26-iRFP in the mice on day 20 after tumor challenge. (C) CT-26 tumor masses were shown on day 15 and 24 after tumor injection. (D) The tumor growth curves of CT-26 mice (n=6 mice, significance was determined by the log-rank test, mean ± SEM ***p <0.01*). (E) Survival rates of mice were shown (n=5 mice in each group).

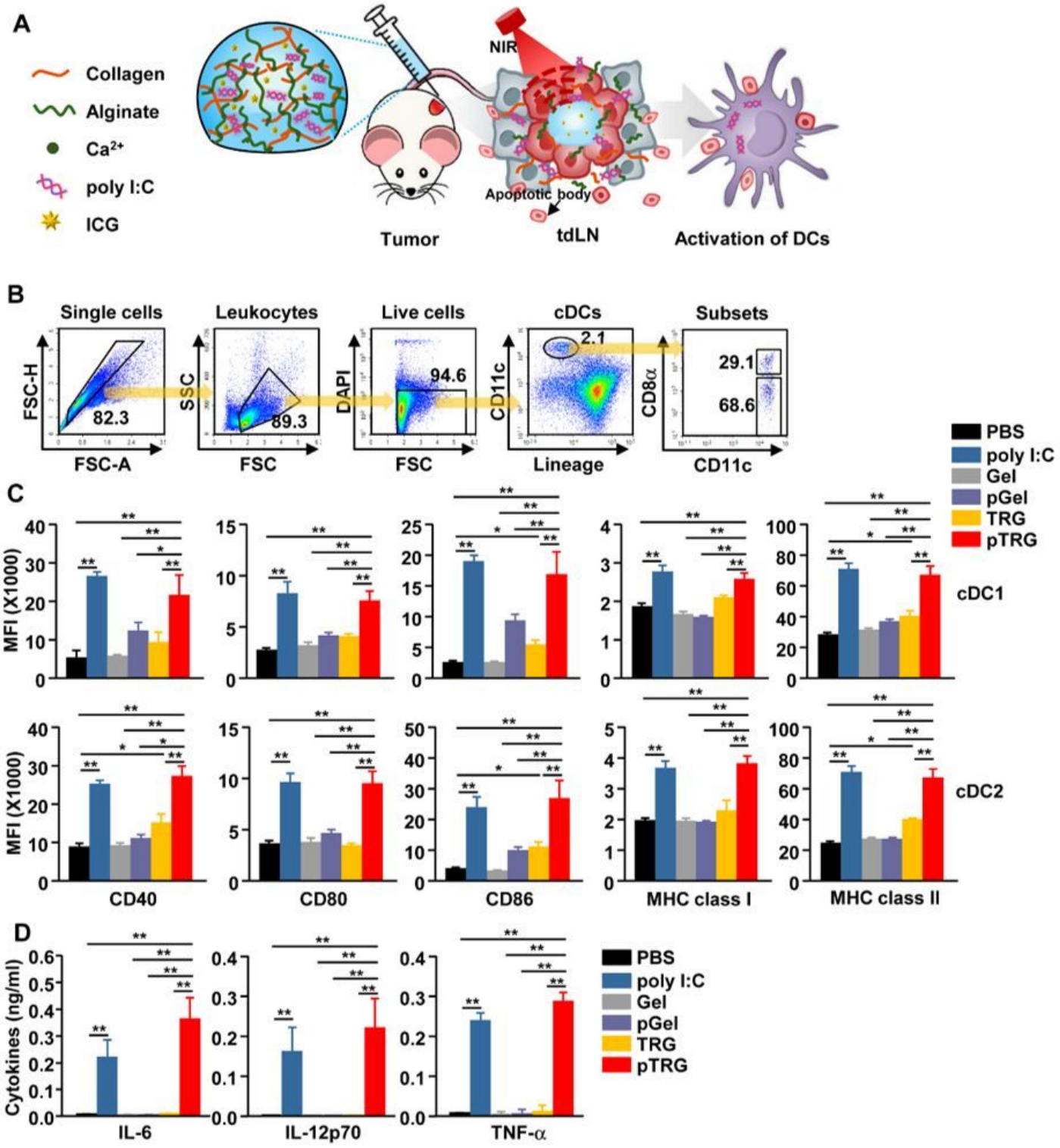

Figure 3

NIR laser irradiation in pTRG-treated tumor induced activation of conventional dendritic cells (cDCs) in tumor draining lymph node (tdLN). (A) Schematic illustration of analysis method for DC activation in the tdLN. (B) Strategy of cDC subsets analysis in tdLN by flow cytometry was shown. (C) The mean fluorescence intensity (MFI) of CD40, 80, 86, MHC class I and II in cDC1 (upper panel) and cDC2 (lower panel) was measured by flow cytometry (n=6 mice, two-way ANOVA, mean ± SEM, *$p < 0.05$, **$p < 0.01$).

(D) Serum concentration of indicated cytokines were analyzed by enzyme-linked immunosorbent assay (ELISA) (n=6 mice, two-way ANOVA, mean ± SEM, **p <0.01*).

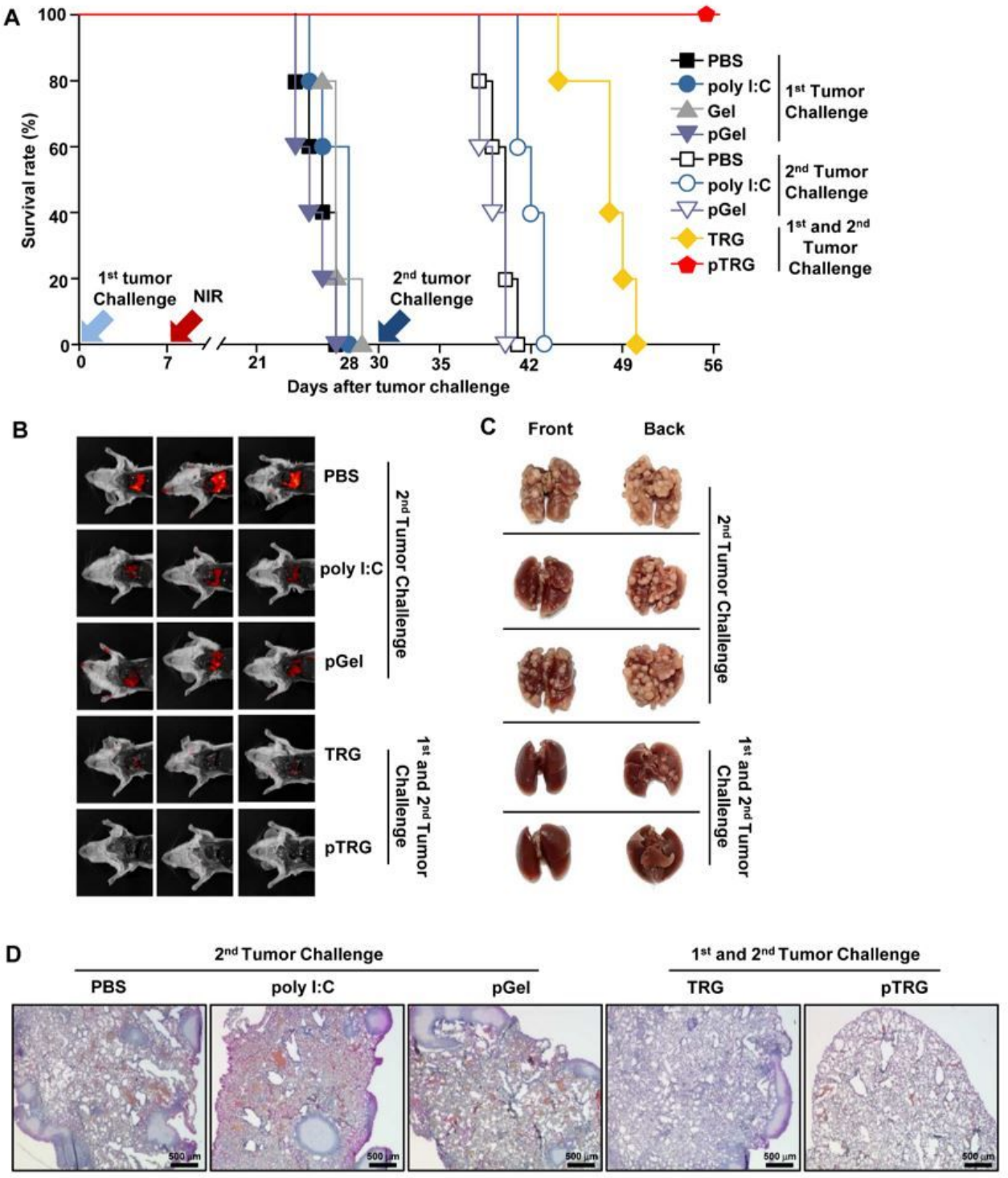

Figure 4

Preventive effect of pTRG from second challenge of CT-26 cell growth in the lung. After first tumor therapy, the survived mice were second challenged intravenous injection with 0.7×10^6 of CT-26-iRFP on day 30 after first tumor injection. (A) Survival rates of the mice were monitored (n=5 mice in each group). (B) Fluorescence image of CT-26-iRFP on day 10 after second CT-26 challenge (n=6 mice). (C) Representative photograph of metastatic lung cancer (n=6 mice). (D) Tumor infiltration was analysed by hematoxylin and eosin (H&E) staining of lung tissue (n=6 mice).

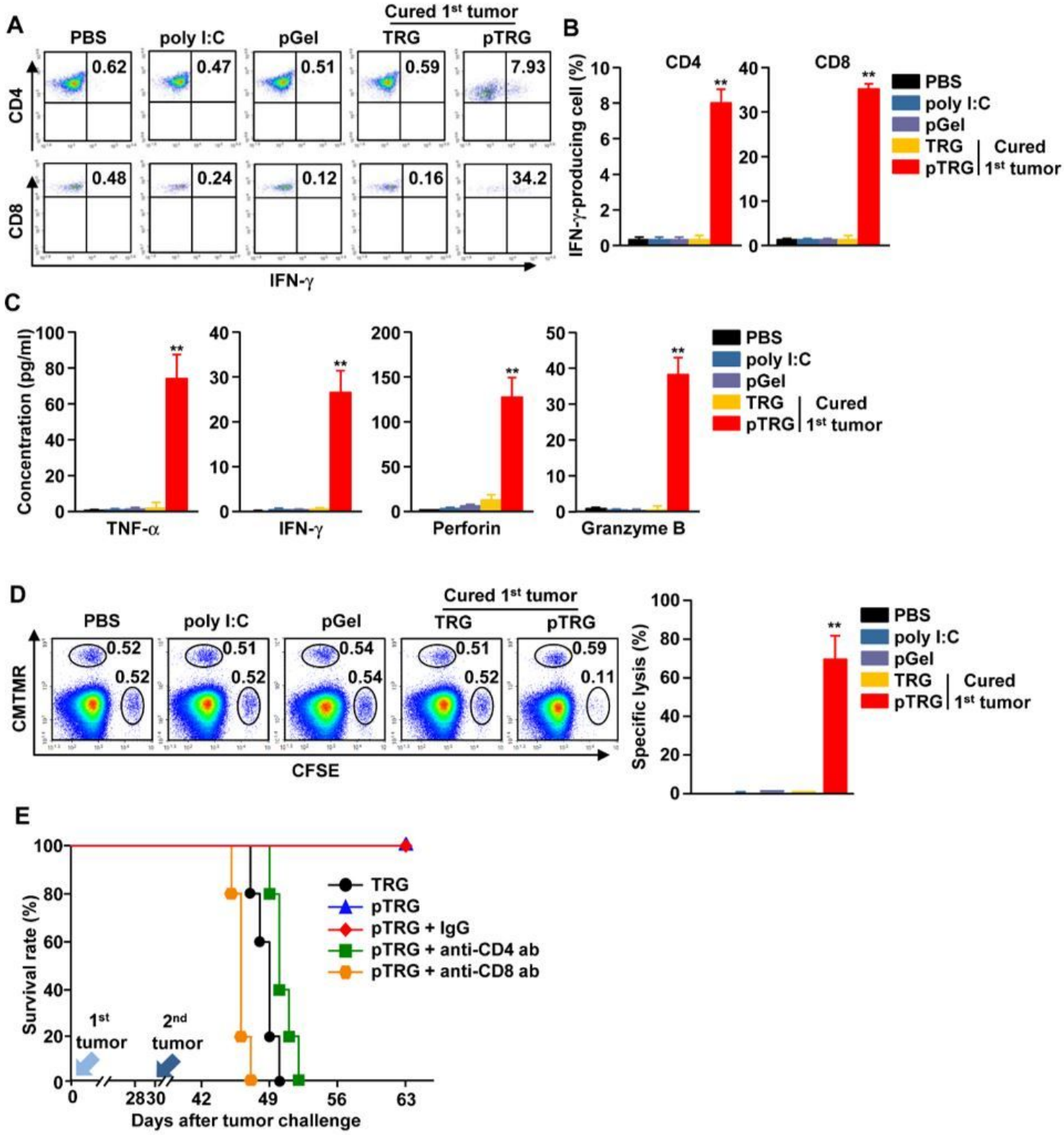

Figure 5

Antigen-specific T cell immunity by pTRG protective mice from second challenge of CT-26. Splenocytes were harvested from mice on day 10 after second CT-26 challenge. The 1 × 10^6 splenocytes were stimulated with 10 μg/mL of CT-26 cell lysate for 24 hours. (A) Intracellular production of IFN-γ in CD4 and CD8 T cells were shown. (B) Mean IFN-γ producing cells in CD4 and CD8 T cells (n=6 mice, two-way ANOVA, mean ± SEM, ***p <0.01*). (C) Concentration of indicated cytokines and cytotoxic mediators in cultured medium was measured by enzyme-linked immunosorbent assay (ELISA) (n=6 mice, two-way ANOVA, mean ± SEM, ***p <0.01*). (D) CT-26 antigen-specific lysis in the mouse *in vivo* were measured by CT-26 antigen-loaded splenocytes transfer. (n=6 mice, two-way ANOVA, mean ± SEM, ***p <0.01*). (E) The mice injected anti-CD4 and CD8 Abs every two days from day 28 of first tumor challenge. The survival rate of the mice was shown (n=5 mice in each group).

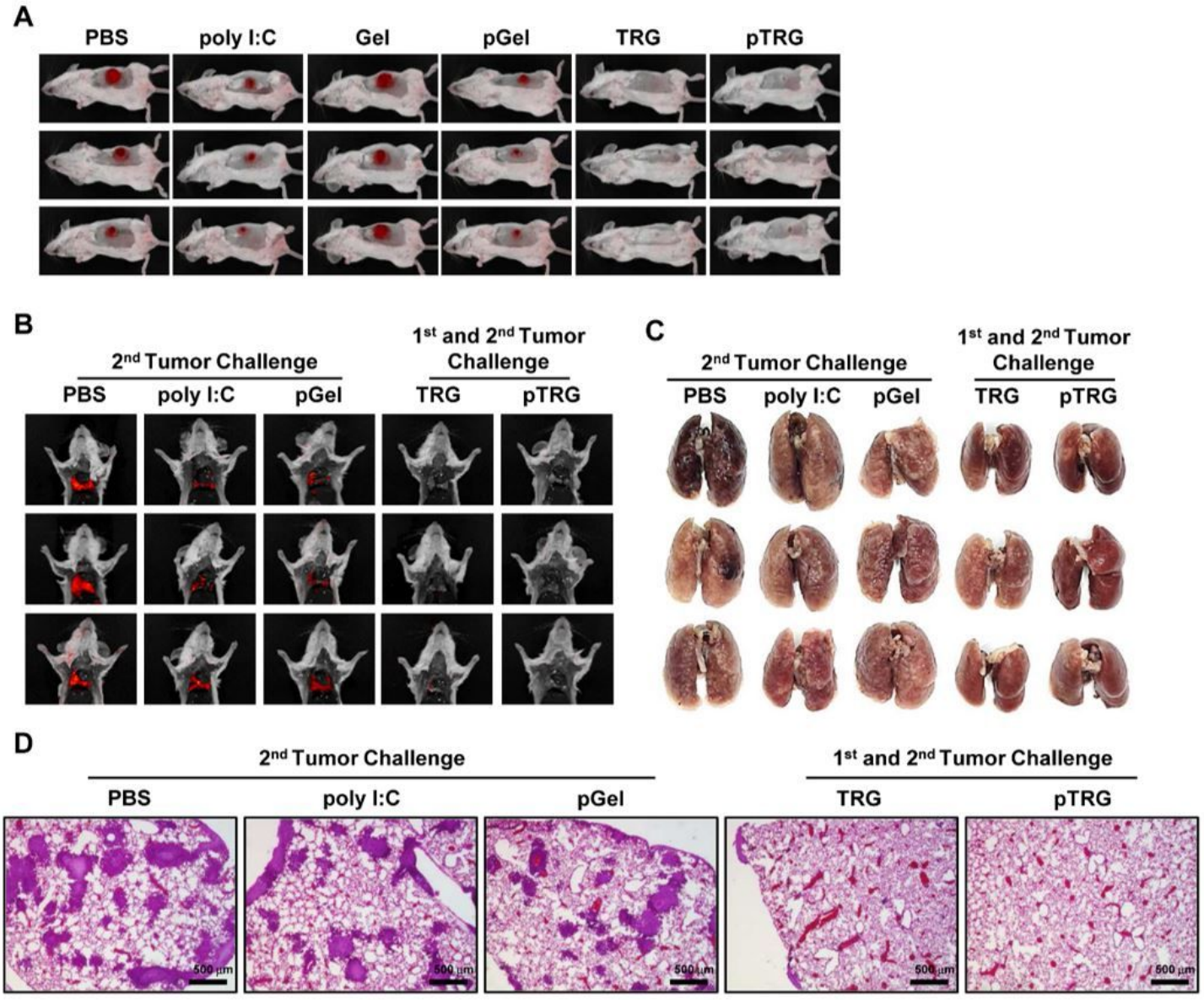

Figure 6

pTRG and NIR laser irradiation prevented 4T1 tumor growth. BALB/c mice were *s.c.* injected with 1×10^6 4T1-iRFP cells. On day 7 after tumor implantation, the mice were *i.t.* treated with PBS, poly I:C, Gel, pGel, TRG, and pTRG with NIR laser irradiation (1.5 W/cm^2, 5 min). (A) iRFP imaging in the 4T1 tumor-bearing mice on day 20 (n=6 mice). (B to D) The survived mice from first 4T1 challenge were given a second challenge of 4T1 (0.5×10^6) cells by intravenous injection on day 30 following the first tumor injection. (B) iRFP fluorescent images and (C) photograph of metastatic lung cancer on day 10 after second 4T1 challenge (n=6 mice). (D) Representative images of hematoxylin and eosin (H&E) staining of lung tissue (n=6 mice).

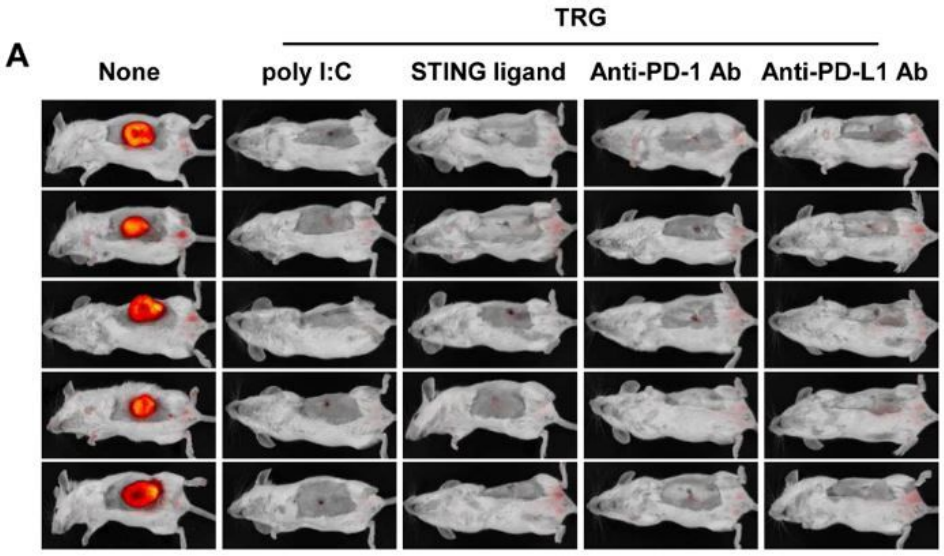

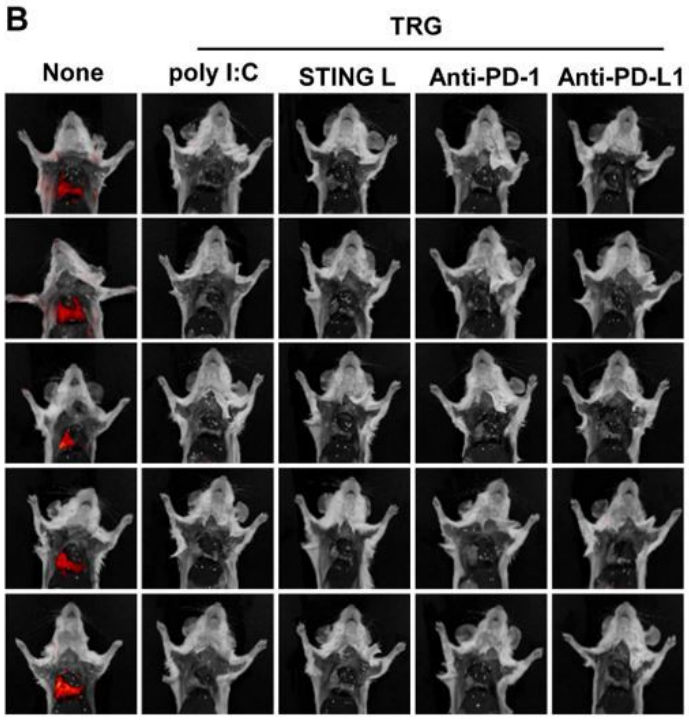

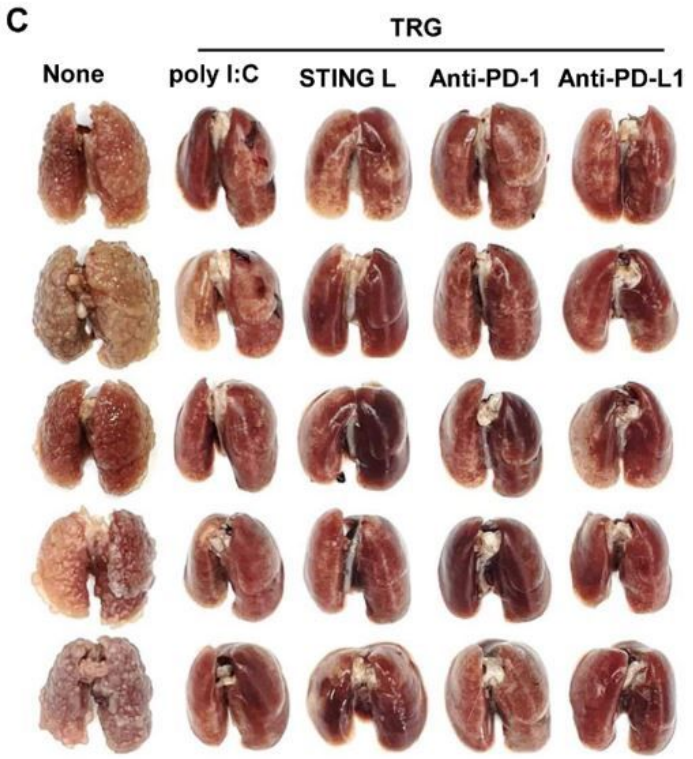

Figure 7

Effect of TRG as cancer therapeutic carrier for immunotherapy. On day 7 after CT-26 tumor implantation, the mice were *i.t.* injected to TRGs contained with PBS, poly I:C, stimulator of interferon genes ligand (STING L), anti-PD-1 antibody (anti-PD-1), and anti-PD-L1 antibody (anti-PD-L1) under NIR laser irradiation (1.5 W/cm^2, 5 min). (A) iRFP imaging in the CT-26 tumor-bearing mice were shown on day 20 after tumor injection (n=5 mice). (B) iRFP fluorescent images and (C) photograph of metastatic lung cancer on day 10 after second challenge (n=5 mice).

Supplementary Files

This is a list of supplementary files associated with this preprint. Click to download.

- TRGSI.docx